Numerical modelling of the out-of-plane response of full-scale brick masonry prototypes subjected to incremental dynamic shake-table tests

[1] Daniele Malomo, corresponding author, email: daniele.malomo@mosayk.it
[1,2] Rui Pinho, email: rui.pinho@unipv.it
[2,3] Andrea Penna, email: andrea.penna@unipv.it

[1] Modelling and Structural Analysis Konsulting (Mosayk Ltd), Via Fratelli Cuzio 42, 27100, Pavia, Italy
[2] Department of Civil Engineering and Architecture, University of Pavia, Via Ferrata 3, 27100, Pavia, Italy
[3] European Centre for Training and Research in Earthquake Engineering (Eucentre), Via Ferrata 1, 27100, Pavia, Italy

ABSTRACT

Structural failure of existing unreinforced masonry buildings, when subjected to earthquake loading, is often caused by the out-of-plane response of masonry walls. Their out-of-plane resistance could vary considerably depending on several factors, such as boundary conditions, vertical overburden and construction technique. Amongst the latter, the cavity wall system, originally introduced in Northwest Europe in the 19th century and then spread to several countries including USA, Canada, China, Australia and New Zealand, has been shown to be particularly vulnerable towards out-of-plane actions. In this work, the use of the Applied Element Method was investigated and subsequently considered for reproducing the experimentally observed out-of-plane shake-table response of unreinforced masonry full-scale cavity wall specimens subjected to both one-way and two-way bending. Finally, given the adequate results obtained and aimed at investigating further both potential limits and actual capabilities of the adopted modelling strategy, the proposed modelling strategy was also extended to the simulation of the dynamic out-of-plane-governed failure mode of a full-scale building specimen tested up to complete collapse.

Author keywords: numerical modelling; applied element method; out-of-plane; shake-table; unreinforced masonry.

INTRODUCTION

The out-of-plane (OOP) failure of unreinforced masonry (URM) elements might cause significant damage due to the separation between transversal and longitudinal walls, as well as the lack or ineffectiveness of the mechanical connections amongst façades and diaphragms, as widely discussed in e.g. [1]. Moreover, it precludes the exploitation of global capacity associated with the in-plane resistance of the structural walls, often leading to early collapse of the structural system (e.g. [2–4]). Notwithstanding the above, relatively limited work has been carried out over the years on the verification and validation of advanced numerical approaches for the modelling of OOP dynamic response of full-scale URM systems. This is probably related to the fact that the necessary experimental data was up until recently not available, with only a few dynamic tests having been carried out (e.g. [5–9]), and confined to the cases of single leaf panels/façades tested in one-way bending conditions. Research on the two-way bending mechanism had instead been limited to quasi-static airbag tests on full-scale specimens (e.g. [6,7]), inclined platforms [8] and dynamic shake-table tests on both reduced-scale [5,9] and full-scale [10,11] brick and stone masonry sub-components. Despite the high vulnerability towards OOP actions typically exhibited by cavity wall systems, instead, no full-scale dynamic two-way bending tests were available in the literature up until the recent works of Graziotti et al. [12] and Tomassetti et al. [13].

From a numerical viewpoint, as shown by Mendes et al. (2007, [14]), the modelling of OOP responses still represents a major challenge, and the use of different approaches may lead to very different results. Amongst others, discontinuum-based models, including the Distinct Element Method (DEM, [15]), proved to be particularly suitable for simulating the behaviour of OOP-loaded masonry assemblies, especially in the case of dry-joint structures (e.g.[16,17]) and reduced-scale mortared-joint components (e.g. [18–20]), possibly up until complete collapse. In this framework, as common practice also among various other interface-based models (e.g. [21–24]), zero-thickness spring layers are often used to describe the interaction between adjacent rigid or deformable bodies, masonry texture, as well as wall section morphology, can be faithfully reproduced accounting for their non-negligible influence on the OOP response of URM panels, as demonstrated e.g. by de Felice [25]. Satisfactory agreement with experimental outcomes has been also reached by various researchers, including e.g. Lemos and Campos Costa [26], who simulated the shake-table response of a full-scale irregular block masonry specimen. Although a simplified joint model was employed for reducing the computational efforts, the overall OOP collapse failure mechanisms were adequately captured by the model. A more detailed modelling strategy was adopted by Galvez et al. [27] for reproducing the shake-table collapse mode of a two-story reduced-scale URM building specimen with periodic brick texture, leading to accurate results despite the very high computational cost required, as noted by the authors.

Within the discrete elements family, the rigid body and spring model (RBSM) [28] proved to be a valid alternative with respect to other micro-modelling methods. According to the RBSM, a masonry assembly is assumed to be composed of rigid blocks connected by discrete deformable interfaces with distributed normal and tangential nonlinear springs, as described in Casolo [29]. Regardless, since the recontact between neighbouring elements (if different from the ones initially set) is not accounted for, the modelling of OOP collapses is unattainable using the standard formulation of RBSM [30]. Thus, additional hybrid computational procedures are currently being explored, as proved by the RBSM/FEM homogenised hybrid model lately developed by Silva et al. [31], which provided a good agreement with quasi-static tests results on URM panels subjected to two-way bending OOP loading, as well as by the work of e.g. Baraldi [32] and Pantò et al. [33]. Meguro and Tagel-Din [34–36] proposed an analogous but more computationally effective approach with respect to the RBSM, the Applied Element Method (AEM), partially overcoming the abovementioned limitations.

(interested readers may refer to Malomo et al. [37] for further details regarding the main differences between the latter approaches). Its formulation allows the reproduction of the structural response both in the finite and discrete domains, taking into account contacts and dynamic element interactions automatically. Moreover, the possibility of describing the interaction between in-plane and OOP actions and the associated cracks propagation with a relatively low computational cost, makes this numerical tool suitable for the simulation of the global response of complex large-scale structures up until complete collapse, as witnessed by some recent applications (e.g. [38–42]).

As a result of the aforementioned features, an implicit AEM-based structural analysis software tool - Extreme Loading for Structures (ASI) [43], has been selected and consequently employed in this work for modelling a series of full-scale URM wall specimens tested under dynamic excitation by Graziotti et al. [12,44], which featured one-way bending, as well as two-way bending response conditions, including single-leaf and cavity walls made of both calcium-silicate (CS) and clay (CL) bricks. Despite the fact that detailed simulations of the dynamic response of such structural systems are needed for the development of seismic risk models in regions where these structures are present (e.g. [45,46]), their numerical assessment under dynamic OOP actions up to complete collapse, as far as the authors' are aware of, has not been addressed yet. The proposed modelling strategy, discussed and described in detail in subsequent sections of this paper, is shown to be able to capture adequately the OOP dynamic response of the different URM walls considered, tested under several combinations of boundary conditions, geometrical configurations and vertical pressures, estimating with relatively satisfactory accuracy both their base shear capacity, as well as failure mode. Finally, given the encouraging results obtained and with a view to scrutinise the applicability of the adopted methodology when considering more complex and realistic interactions among OOP-loaded components and adjacent elements, the simulation of the OOP-governed collapse mode of a shake-table-tested full-scale cavity wall building prototype is also presented.

THE APPLIED ELEMENT METHOD FOR MASONRY STRUCTURES

According to the AEM, which general formulation is discussed in detail in e.g. [34], a masonry element is idealised as an assembly of rigid units (where mass is concentrated) connected by zero-thickness springs, in which the material properties of the unit-mortar interface are lumped. In **Fig1.(**a), this simplified micro-modelling strategy is applied to the representation of the interaction among contiguous units of an arbitrary masonry segment. (as a proof of concept, however, it is noted that in the latter, finite thicknesses - which do not necessarily represent the actual ones - have been depicted).

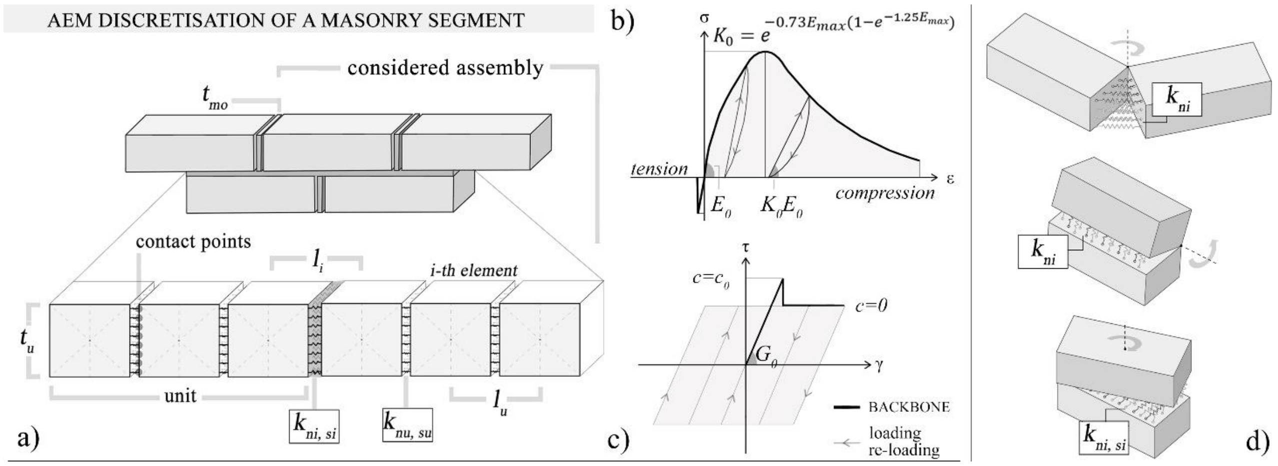

Fig. 1 (a) AEM discretisation of a masonry segment, springs models under (b) normal and (c) shear cyclic loading; (d) AEM deformed shapes due to flexural and torsional actions; adapted from [37]

Unit and interface springs are supposed to be arranged in series, as it can be gathered also from **Eq. (1)**, where l_i is the centroid to centroid distance among adjacent units, t_{mo} is the actual thickness of mortar bond, t_u stands for unit thickness, d is transversal spring spacing (i.e. the spacing between each normal/shear spring, which are located at the same contact point) and E_u, G_u, E_{mo} and G_{mo} are unit and mortar Young's and shear moduli, respectively. Unit deformability can be also accounted by introducing internal subdivisions to which are assigned springs characterised by the stiffnesses (i.e. k_{nu}, k_{su}, see **Eq. (2)**), where l_u is centroid-to-centroid distance among elements forming the unit (in this case, because the elements are the same size and given that zero-thickness spring layers are used, l_u is equal to l_i).

$$k_{ni} = \left(\frac{l_i - t_{mo}}{E_u\, d\, t_u} + \frac{t_{mo}}{E_{mo}\, d\, t_u}\right)^{-1}, \quad k_{si} = \left(\frac{l_i - t_{mo}}{G_u\, d\, t_u} + \frac{t_{mo}}{G_{mo}\, d\, t_u}\right)^{-1} \quad \textbf{(1)} \quad k_{nu} = \left(\frac{E_u\, d\, t_u}{l_u}\right), \quad k_{su} = \left(\frac{G_u\, d\, t_u}{l_u}\right) \quad \textbf{(2)}$$

As already mentioned, when employing AEM, each component of a given masonry element (i.e. units and mortar) needs to be described in terms of its mechanical properties. However, experimental campaigns on masonry elements rarely involve tests that would allow one to obtain all necessary material characterisation for unit and mortar separately. Thus, undertaking the approach proposed in Malomo et al. [47], a number of formulae inferred through empirical (i.e. [48,49]) and theoretical (i.e. [50–53]) investigations were used to obtain first estimates of the required material parameters where direct experimental values were not available. Then, the ensuing average is considered for modelling purposes and the associated shear moduli are obtained assuming material isotropy.

The CS and CL bricks tensile strength, on the other hand, was estimated assuming the 5% and 15% of their compressive strength respectively, as proposed by Malomo et al. [54]. These values will be given in the next sections, together with the experimental ones. While a cut-off criterion is employed for spring tensile failure, a simplified version of the elastoplastic fracture model proposed by El-Kashif and Maekawa [55] is commonly used for simulating the cyclic cumulative damage of masonry elements subjected to uniaxial compression (see **Fig. 1**(b)), where the initial Young's modulus E_0, the compressive plastic strain ε_p and the fracture parameter K_0 (which represents the extent of the internal damage) define the envelope for compressive stresses. The latter is determined during the analysis as an exponential function of the maximum equivalent strain E_{max}, and controls stiffness and strength deterioration under repeated loading and unloading cycles. On the other hand, the hysteretic constitutive law that governs the cyclic response of shear springs is based on a Mohr-Coulomb yielding criterion, where cohesion is set to zero right after reaching the maximum shear strength, as depicted in **Fig. 1**(c), where G_0 stands for shear modulus. As proposed by [56] for the analysis of the rocking-dominated response of classical column systems, no artificial (external) dynamic relaxation schemes were introduced, meaning that the only source of damping in the proposed numerical models is the energy dissipation due to difference in loading and unloading paths of compression springs, as well as that induced by the process of crack closure/opening. As witnessed by recent applications (e.g. [38,57]), this usually provides adequate results also when considering OOP-governed failure mechanisms of both URM components and building prototypes. Interested readers may refer to Tagel-Din [58] for additional details. For what concerns the modelling of collision phenomena, as further discussed in e.g. [59], it is worth mentioning that when considering two elements initially not in contact, *impact springs* are automatically generated at the interface only when collision takes place, where the impulsive response is governed by the material with lower stiffness, thus enabling to represent progressive collapse modes in a reasonable timeframe. When simulating OOP modes, as further discussed in the subsequent sections, joint failure modes, which often induces flexural and torsion local stresses, can be accounted by normal and shear spring respectively, as illustrated in **Fig. 1**(d).

First Verification of AEM with Material Characterisation Tests

In this subsection, a first comparison between experimental and numerical outcomes is proposed with a view to assess the AEM capabilities in reproducing the main OOP local failure mechanisms. To this end, the results of characterisation tests on small-scale specimens carried out by Graziotti et al. [12] were selected and consequently replicated using the AEM. Bond-wrench and torsion-compression tests on both CS and CL brick masonry samples, as well as four-point bending tests on CS wallettes (experimental data were not available for CL wallettes), were considered in such modelling exercise. The CS brick masonry specimens were characterised by a single-leaf stretcher bond arrangement of 212×103×71 mm units and 10 mm thick mortar joints. The same mortar bond thickness and pattern was also employed to assemble the 208×98×50 mm CL brick masonry specimens. In **Table 1**, the considered masonry material properties (fc_m and fc_u are masonry and unit compressive strengths, f_w is bond tensile strength, c is cohesion and μ is friction coefficient) are reported:

Table 1 Experimental [12] and inferred material properties of both CS and CL brick masonry

	CS - δ_m = 1833 [kg/m^3]								CL - δ_m = 2000 [kg/m^3]							
	fc_m	fc_u	f_w	E_m	c	μ [-]	E_u	E_{mo}	fc_m	fc_b	f_w	E_m	c	μ [-]	E_u	E_{mo}
Avg [MPa]	8.5	15.3	1.0	5430	0.8	0.5	14275	1297	4.5	46.8	0.4	6798	0.2	0.6	17550	1580
C.o.V. [%]	7.8	6.1	18.2	31.2	-	-	-	-	8.5	11.0	55.3	23.3	-	-	-	-

The comparison between experimental and numerical results shown in **Fig. 2** seemed to indicate that the main local OOP failure mechanisms can be adequately predicted using the considered computational method. Indeed, a good agreement in terms of overall capacity was found for the case of torsion and four-point bending tests, albeit the residual strength was not fully captured by the models. This latter aspect is due to the fact that, when a given spring fails in tension, its stiffness is set to zero in the subsequent steps, causing a sudden loss of capacity right after the strength peak. For what concerns the four-point bending tests, the models predicted a rather brittle response, with the formation of the cracks in the constant moment zone and instantaneous failure, which appears in line with experimental results on these specific masonry types (see e.g. [60]).

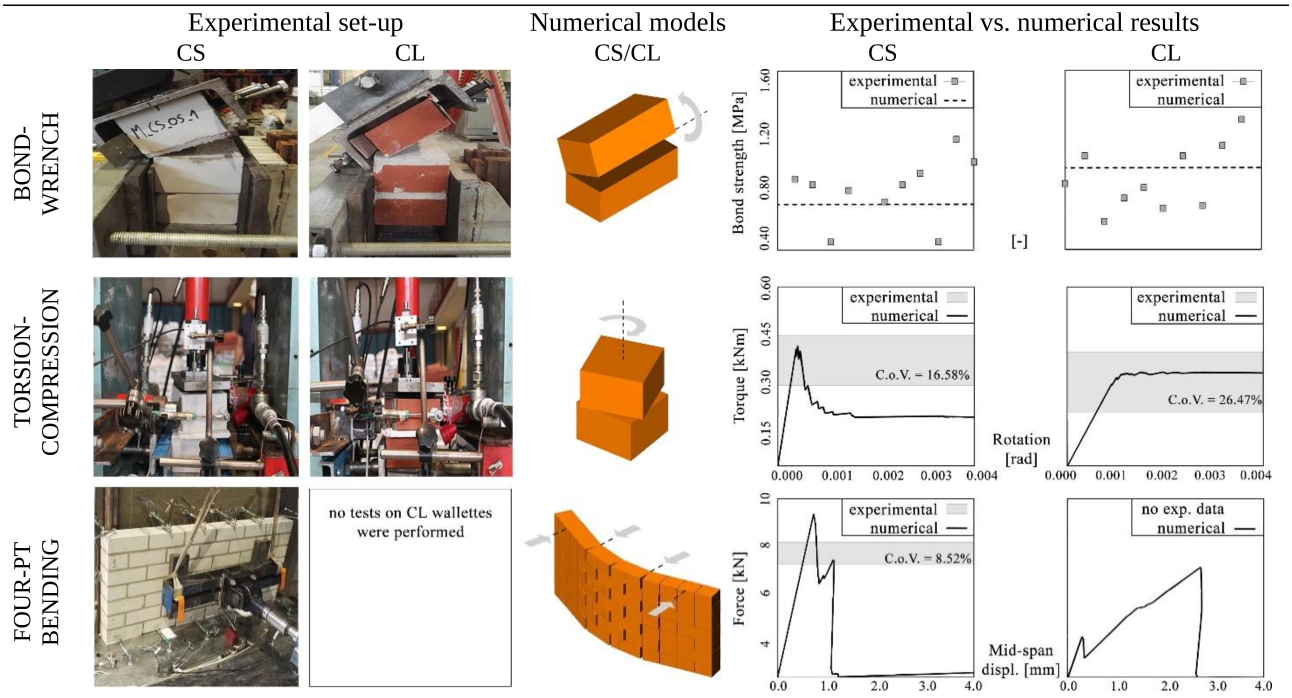

Fig. 2 Comparison between experimental [12] and numerical results (top to bottom): bond strength vs. tested samples, applied torque vs. rotation and maximum load at failure vs. mid-span displacement

SIMULATION OF SHAKE-TABLE OUT-OF-PLANE TESTS ON WALL COMPONENTS

As mentioned previously, a series of somewhat pioneering OOP shake-table tests [44,61] was recently performed at the Eucentre laboratory (Pavia, Italy) involving both single-leaf CS and CL brick masonry panels as well as cavity CS-CL walls. The latter are typically constituted by the assembly of a loadbearing inner CS leaf plus an outer CL veneer with only aesthetic and insulation functions, weakly coupled by metal connectors (tie elements) characterised by a “zigzag” end shape embedded within the CS bricks and an L-shaped extremity embedded on the CL panels. The considered specimens were tested dynamically under different boundary conditions and ties distribution, in both one-way and two-way OOP bending conditions. The employed bricks, whose dimensions were 212×103×71 mm and 208×98×50 mm for

CS and CL brick masonry respectively, were arranged according to a stretcher bond pattern, while the mortar layers thickness was approximately 10 mm for all the specimens. Further information on the loading protocols and experimental results (available from *http://www.eucentre.it/nam-project*, see also Tomassetti et al. [62] will be briefly presented in the next sub-sections, while full details on the tests may readily be found in Graziotti et al. [44,61].

As observed in **Fig. 3**(a), for both sets of tests, a rigid steel frame ensured that the dynamic input motion from the shake-table was transferred from the table to the top of the wall with negligible amplification. Further, the connection between frame and the beam on top of the specimens consisted of a pair of steel braces with mechanical hinges at one end, while, in the case of the U-shaped walls subjected to two-way OOP bending conditions, steel profiles were also used to clamp the free extremities of the return walls (herein modelled as a linear elastic beam rigidly attached to the return walls). With a view to decrease the computational burden, the frame system has been idealised as a fixed linear elastic beam, to which the walls were connected by means of horizontal rigid link elements. The same seismic input that was introduced at the foundation level was then also applied to the beam, thus simulating the acceleration time-history transmission to the top beam with negligible amplification that took place during the tests, while assuring compatible boundary conditions. Contrarily, both loading and foundation beams were explicitly modelled, assuming a linear elastic response. Rigid link elements, connecting the top and the bottom beams, were again used here to apply the vertical stress; initial pre-stresses, depending on the considered overburden, were assigned to the link elements reproducing the experimental ones. Further, and in order to replicate the actual stiffness of the springs employed during tests (connecting the steel top beam to the RC foundation), an equivalent Young's modulus was computed (assuming an average link section of 100 mm^2) and subsequently allotted to the vertical links.

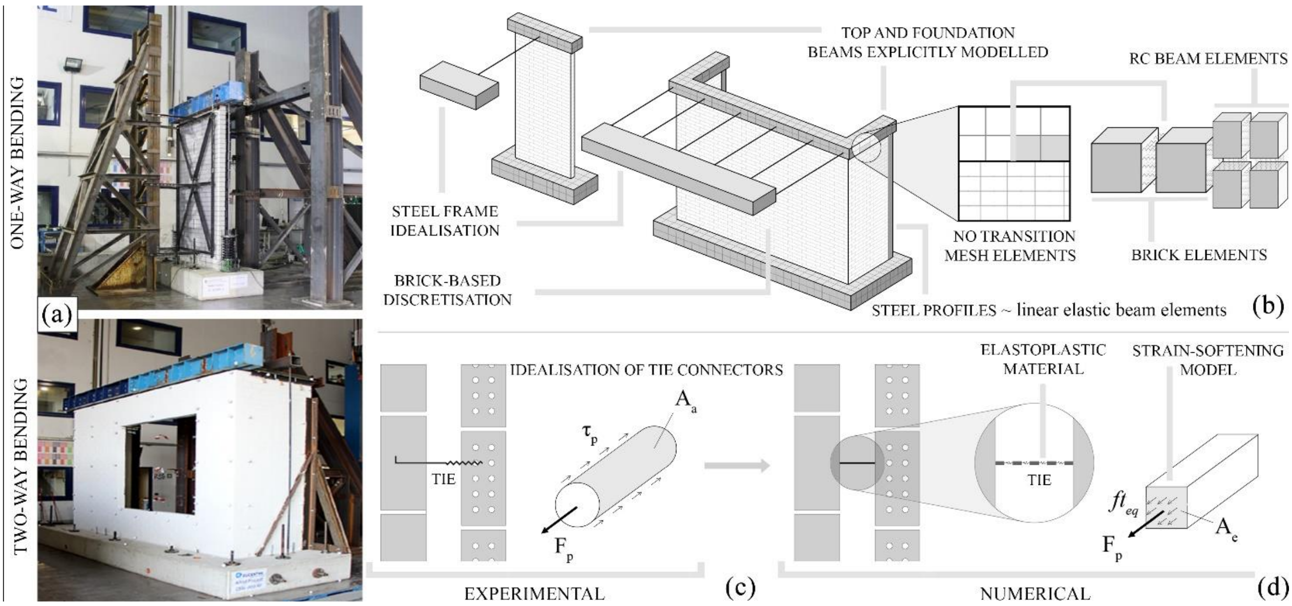

Fig. 3 (a) Test layouts [12,44], (b) numerical idealisation and mesh discretisation approach, (c) experimental and (d) numerical ties configuration, (e) stress-strain relationship of CL wall-to-tie interface

As shown in **Fig. 3**(b), a coarser mesh was assigned to the beams, since the AEM does not require mesh transition from large to small-size elements and partial connectivity between units is possible.

Each surface of a given rigid element (both in case of RC and URM mesh units) was connected to the adjacent one by means of 25 springs. The URM panels were discretised through a brick-based mesh, reproducing the experimental arrangement of bricks accurately. An additional discretisation was then applied to subdivide each element along the vertical axis for better capturing their potential flexure and shear failure when such modes were observed experimentally (e.g. four-point OOP bending test specimen, two-way bending central panel). For what concerns the tie–wall interfaces, it is worth noting that, despite recent experimental developments [12] showing that these elements might provide sufficient coupling of the horizontal displacement of the two leaves in case of dynamic loading, a reliable method for quantifying this phenomenon at the joint level has not been proposed yet. Thus, considering that experimental evidence [63] showed that they typically fail in the middle of the CL mortar bonds (see **Fig. 3**(c)), the idealisation depicted in **Fig. 3**(d) has been adopted, whereby the contact between masonry and ties occurs only through the transverse section of the ties (i.e. the ties' length is equal to that of the cavity). This is because the modelling of interpenetration phenomena between elements (such as the pull-out) would imply a very high computational burden; amongst other things, the number of dynamic contacts would increase considerably. Consequently, the adhesion stresses $\tau_p = 4.28$ MPa (which can be quantified dividing the associated pull-out force F_p by the embedded perimeter surface of the ties A_a), mobilised throughout $A_a \sim 534$ mm^2 were in the models replaced by equivalent stresses $ft_{eq} = (\tau_p \times A_a)/A_e$ developed on the transverse section of the ties ($A_e \sim 9$ mm^2). The spring layer between CL walls and ties (modelled as 3D beam elements with elastic-perfectly-plastic behaviour and pull-out ultimate strength F_p equal to the experimentally-measured one, i.e. 2.29 kN) was characterised by a strain-softening constitutive law (see **Fig. 3**(d)), with a maximum tensile strength of ft_{eq} and a very low residual value (i.e. $0.05ft_{eq}$) representative of the post-peak resistance observed experimentally [63], while a linear elastic connection between CS walls and ties, was employed.

One-Way Bending Tests

Two different types of full-scale specimens were tested dynamically, in their OOP one-way bending conditions, by Graziotti et al. (2016). The acronym assigned to each prototype indicates the structural type considered (i.e. CS single leaf, SIN, and complete cavity wall systems, CAV), the imposed vertical pressures σ_{vOOP} (i.e. 0.10-0.30 MPa) and the extent of ties/m^2 respectively (i.e. 0.0, 0.2, 0.4 ties/ m^2). The first one (i.e. SIN-03/01-00) consisted of a single leaf wall made of CS bricks. The remaining specimens (i.e. CAV-01-02, CAV-03-02 and CAV-01-04), instead, were constituted by an inner CS brick masonry load-bearing panel (1.44x0.102x2.75 m) coupled with an outer veneer in CL bricks (1.43x0.100x2.70 m); the distance between the two leaves was approximately 80 mm, as typical in construction practice. The main masonry properties are reported in **Table 2**:

Table 2 Experimental [44] and inferred material properties of both CS and CL brick masonry

	CS - δ_m = 1833 [kg/m^3]								CL - δ_m = 2000 [kg/m^3]							
	fc_m	fc_u	f_w	E_m	c	μ [-]	E_u	E_{mo}	fc_m	fc_u	f_w	E_m	c	μ [-]	E_u	E_{mo}
Avg [MPa]	6.2	18.7	0.2	4182	0.2	0.4	6628	1772	11.2	46	0.2	6033	0.2	0.5	17179	1971
C.o.V. [%]	7.0	13.7	16.3	33.3	-	-	-	-	7.4	11.2	60.1	25.4	-	-	-	-

Different levels of vertical overburden were imposed on the CS piers through a steel beam placed on the top of the CS walls and pulled down by means of two steel rods in series with a couple of springs characterised by a stiffness *k*. Such system assures constant pressure on the masonry panels whilst imposing also the envisaged double-fixed boundary conditions. It is noted that in case of SIN-03/01-00, the experimental procedure consisted of two main stages; initially considering an overburden pressure of 0.3 MPa, and then decreasing it to 0.1 MPa with a view to induce the collapse of the specimen. As discussed in Graziotti et al. [44], three main input motions (see **Fig. 4**(a)) were selected, scaled and incrementally imposed to the specimens until collapse. The first one, *Gr1*, corresponded to an accelerogram compatible with the probabilistic seismic hazard assessment for the Groningen region (see [64]) available at the time of the tests (PTA – i.e. peak table acceleration – equal to 0.25g, herein scaled from 10 up to 400%), whereas the second one, *Gr2*, was obtained by numerical simulation of first story motion of a typical terraced house (PTA equal to 0.47g, scaled during tests from 60 up to 200%) using a calibrated TREMURI [65] model. A further input signal employed is a 2 Hz Ricker Wave Acceleration input (*RWA*), which consists of a particular acceleration pulse (PTA ranging from 0.21 up to 1.88g, depending on the specimen).

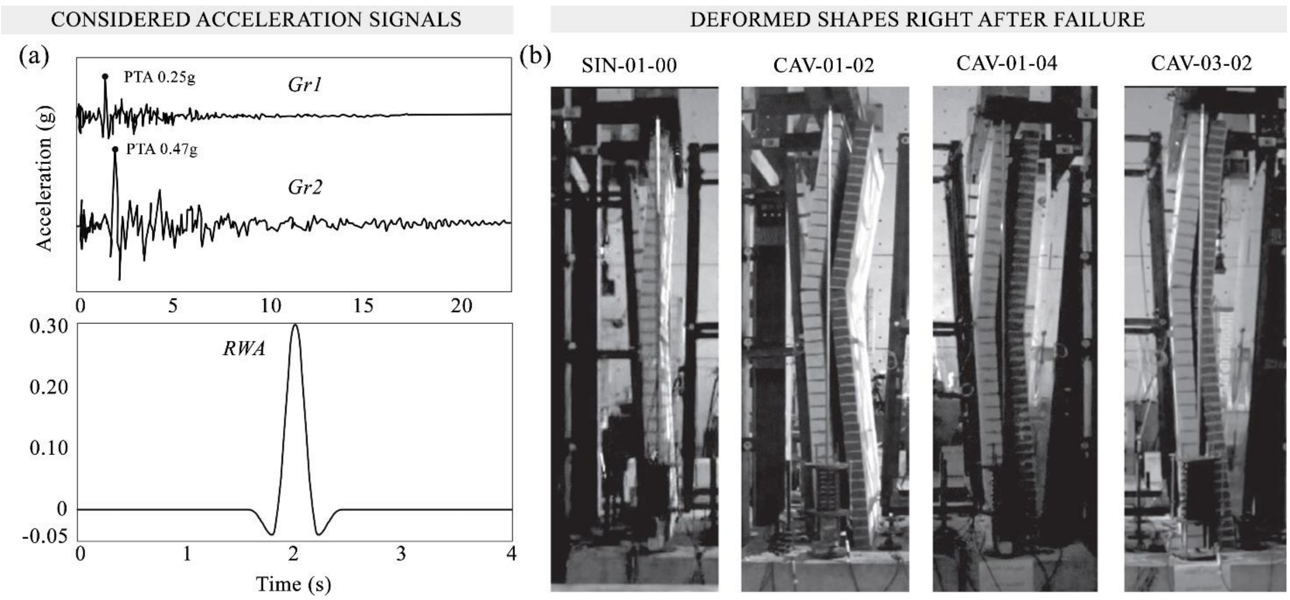

Fig. 4 (a) *Gr1*, *Gr2* and *RWA* signals, (b) snapshots of selected specimen failures (adapted from [44])

All the walls, as depicted in **Fig. 4**(b), exhibited rocking behaviour with the formation of horizontal cracks at the walls bottom, top and around mid-height (MH) sections (this is the reason why, in the models, a brick-based mesh, i.e. without vertical subdivisions, was adopted). All of them, after cracking, reached the OOP collapse for a value of PTA slightly higher than that triggering the activation of the OOP failure mechanism one, as noted by Tomassetti et al. [66], except for SIN-03/01, for which collapse was reached under an overburden (0.30 MPa) different from the value (0.10 MPa) present when the failure mechanism was first activated.

In **Fig. 5**(a)(b)(c)(d), experimental and numerical crack patterns, failure modes, and the relation between horizontal displacement at MH and total horizontal force, are shown together with the numerical progressive collapse of one of the considered specimens (i.e. CAV-01-04, see **Fig. 5**(d)). Following an analogous approach to that suggested in the dedicated experimental paper (i.e. [44]), the experimental force has been obtained by multiplying the absolute acceleration of the centre of mass of the two bodies (idealised as rigid) by the related masses, whilst the displacement is the one relative to the mid-height hinge location, assuming a triangular distribution of the relative acceleration along the wall height (i.e. with maximum acceleration at mid-height hinge location). Since experimental collapse tended to occur slightly later than what was numerically predicted, only the cycles up until numerical collapse were depicted in the hysteretic curves, for a more readily interpretation of the plots.

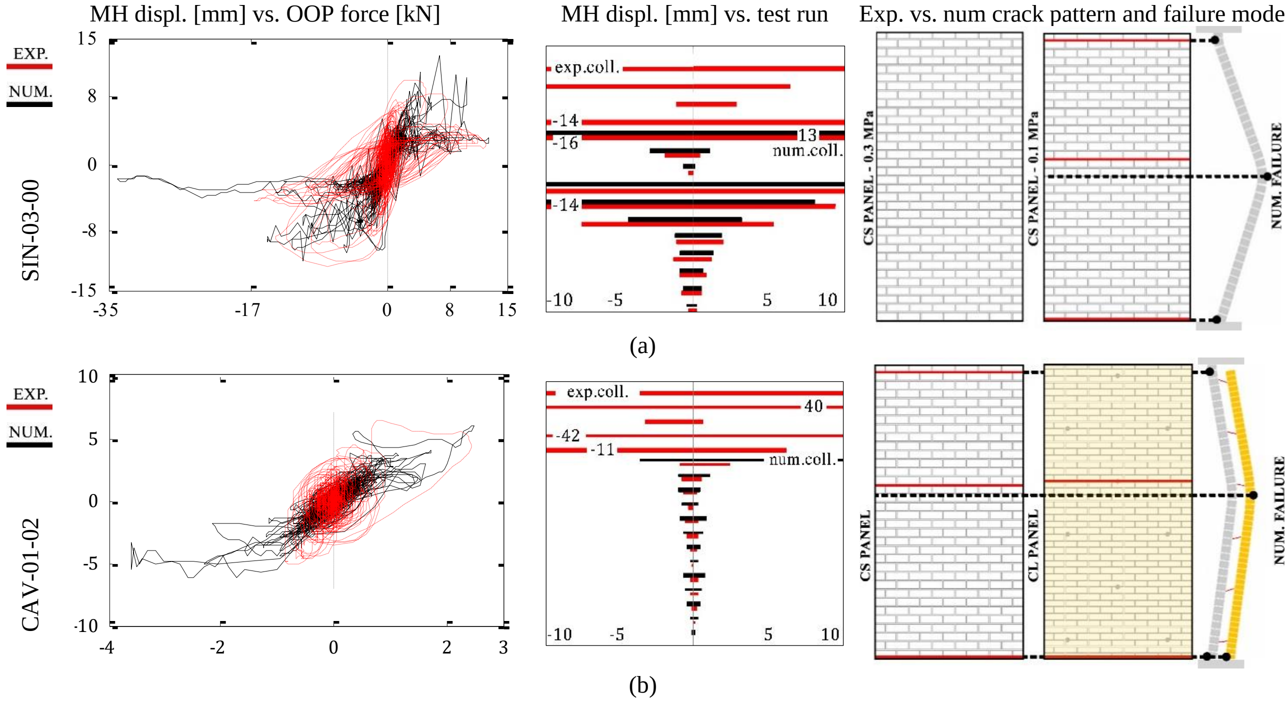

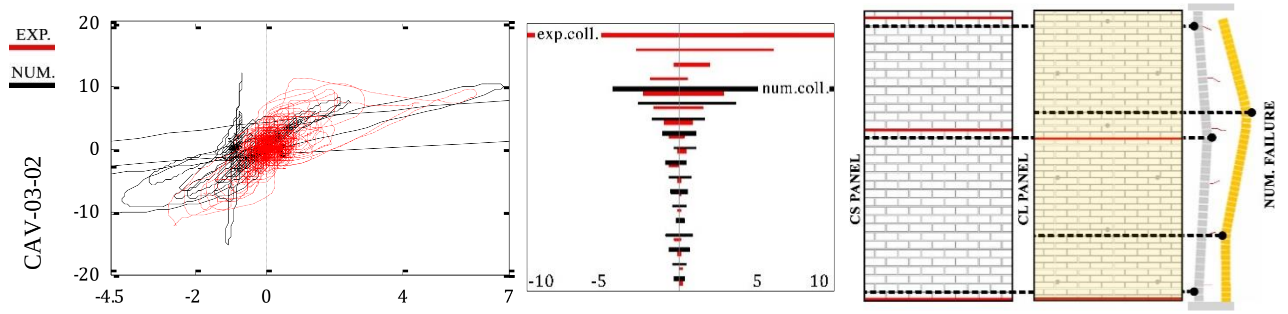

(c)

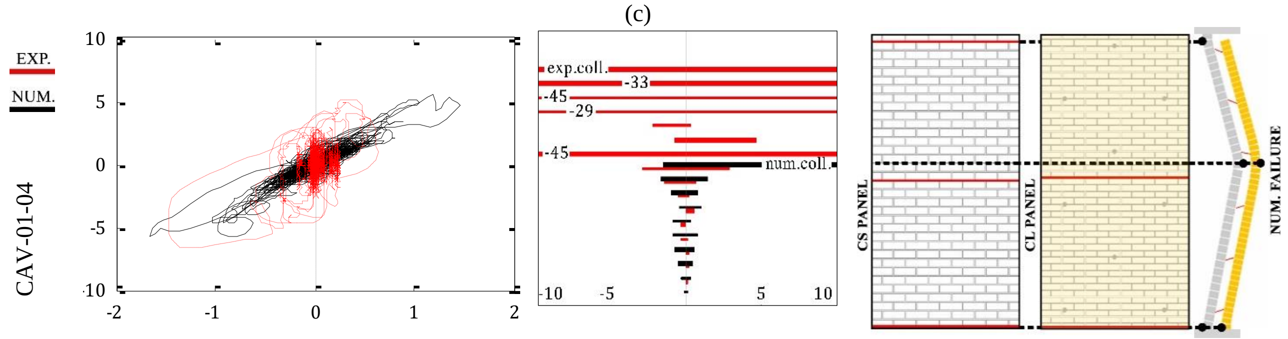

(d)

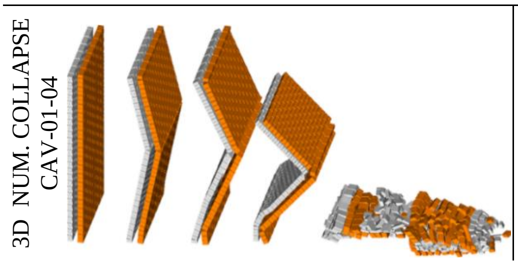

(e)

Specimen ID	Exp. mech. activation PTA [g]	Num. mech. activation PTA [g]	Exp. mech. collapse PTA [g]	Num. mech. collapse PTA [g]	Analysis time [h]
SIN-03-00	0.96	0.96	0.85	0.98	0.8
CAV-01-02	0.50	0.60	0.68	0.63	1.2
CAV-03-02	0.75	0.93	1.11	0.97	1.1
CAV-01-04	0.63	0.67	0.68	0.68	1.4

(f)

Fig. 5 (a)(b)(c)(d) Exp. [44] vs. num. results: hysteretic behaviour, MH displacement for each test run, crack pattern; (e) numerical collapse of CAV-01-04, (f) exp. vs. num. activation mechanism and collapse PTA, required analysis time (note: the colour used for the walls changes as a function of the wall material, where CS is grey and CL is orange)

The dynamic OOP one-way bending of masonry walls is a rather complex response mechanism. Hence, numerical prediction of its hysteretic behaviour and collapse capacity is inevitably and unavoidably challenging. Within such context, therefore, it is felt that the comparisons depicted below can be considered as encouraging, with the numerical models producing results that appear to be within the range of their experimental counterparts. Such a positive impression is further confirmed by what is shown in **Fig. 5**(f) where it can be observed that the estimated values of PTA feature differences with respect to the experimental observations in the range of 7-15%.

Nonetheless, as can be gathered by comparing the numerical PTA associated to the mechanism activation and the one corresponding to collapse (see **Fig. 5**(f)), the model struggled to capture the slight residual resistance exhibited by the specimens after the attainment of the first MH crack. This might be attributable to the simplified tension cut-off criterion implemented in the employed AEM-based code, according to which the interface strength is automatically set to zero after reaching the maximum input value and thus neglecting any residual capacity. This aspect, as discussed in the next subsection, is less evident in the case of two-way bending. Indeed, in such cases, since multiple failure surfaces are involved in the mechanism activation, the failure of a single spring layer does not necessarily induce global collapse. For future comparisons, the computational time required for performing the whole incremental dynamic analysis for each specimen (using a high-performance workstation with CPU Intel Core i7 7820x, 64GB DDR4, SSD M2-960-EVO), is also reported in **Fig. 5**(f), where the observed differences are directly related to the number of degrees of freedom and units/springs involved in the predicted collapse mechanism.

Two-Way Bending Tests

Five different full-scale U-shaped walls, herein all reproduced numerically, were tested by Graziotti et al. [12] under two-way bending conditions at the laboratory of Eucentre. All the specimens were constituted by an assembly of three 2.8 m high URM panels: two return walls (1.1 m long) parallel to the direction of shaking and a main panel (approximately 4 meters long) excited in the OOP direction. The considered masonry properties are those reported in **Table 1**. The nomenclature assigned to each prototype indicates both the masonry type used (i.e. CS and CL) and the vertical pressures $\boldsymbol{\sigma_{vOOP}}$ imposed to the central OOP panel (i.e. 0.05-0.10-0.00 MPa), as well as the applied horizontal boundary conditions, namely restrained-restrained (RR) and restrained-free (RF). Moreover, unless otherwise stated, 0.05 MPa of compressive pre-stress $\boldsymbol{\sigma_{vRET}}$ was applied to the return walls. With respect to the first wall tested (i.e. CS-010-RR/CS-005-RR), the initial $\boldsymbol{\sigma_{vOOP}}$ of 0.10 MPa, in this specific case equal to $\boldsymbol{\sigma_{vRET}}$, was decreased to 0.05 MPa with a view to induce visible OOP damage. The second specimen (i.e. CS-000-RF), only differed from CS-005-RR in the boundary conditions considered (i.e. RF instead of RR), whilst CSW-000-RF was characterised by the presence of an opening (1988×1630 mm) located asymmetrically in the main panel. The fourth specimen (i.e. CL-000-RF) was made of CL bricks, whilst the last prototype tested (i.e. CV-000-RF) was representative of a complete cavity wall system. The distance between the two parallel masonry leaves was approximately 86 mm, and their connection was provided by 0.2 steel ties/m^2. The panels were subjected to a series of dynamic inputs of increasing intensity, up to full collapse of the specimen, considering the four different input motions (i.e. *FHUIZ-DS0, FEQ2-DS3, FEQ2-DS4* and *SSW*, **see Fig. 6**)

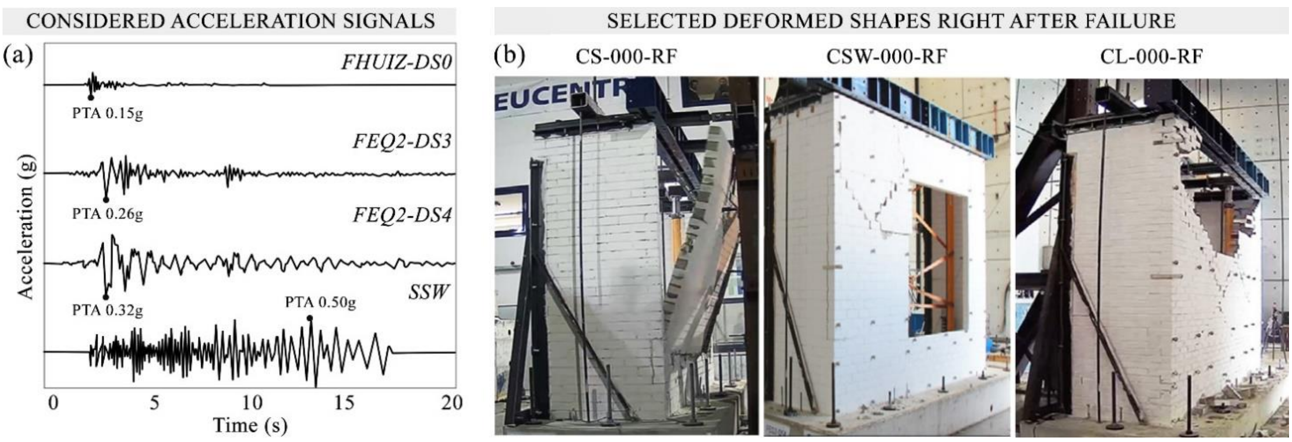

Fig. 6 (a) *FHUIZ-DS0*, *FEQ2-DS3*, *FEQ2-DS4* and *SSW* acceleration time histories, (b) snapshots of selected specimen failures (adapted from [12])

As discussed in Kallioras et al. [67], *FHUIZ-DS0* (PTA equal to 0.15g, scaled from 50 up to 150%) was the second-floor acceleration time-history obtained from a calibrated numerical model of a full-scale building prototype [68] when subjected to the ground motion recorded at Huizinge, The Netherlands, on 16th April 2012. *FEQ2-DS3* and *FEQ2-DS4* (PTA equal to 0.26g and 0.32g, scaled from 50 up to 125% and from 100 to 400% respectively, depending on the considered specimen) correspond to experimentally recorded second-floor acceleration time-histories of the full-scale house when subjected to ground-motion *EQ2* (PTA 0.17g, see [69]) scaled up to 125% and 200%, respectively. A fourth artificial input signal (*SSW*, PTA equal to 0.50g), characterised by a wide spectral shape and long duration, was also employed in order to induce a collapse of specimen CS-005-RR, which otherwise would require unrealistic scaling of the previously introduced floor motions.

In addition to the main modelling assumptions reported at the beginning of this section, the following is also of relevance:

- Experimental collapses were often caused by hybrid modes, i.e. involving both joint and unit failure. Thus, an additional vertical discretisation of the bricks was assigned to the elements of the central OOP panel, whilst a brick-based standard mesh has been allotted to the return walls.
- OOP displacements were evaluated at MH and on the top of the central panel, depending on the considered boundary conditions (i.e. RR or RF), time-histories of inertial forces were computed numerically by multiplying the acceleration recorded at massless small rigid element locations (idealised as lumped in the element centroids) with a tributary mass assigned to them, equal to the one reported in Graziotti et al. [12].

  Finally, the mechanical contribution of tie connectors was accounted for by undertaking the same modelling approach employed for the models subjected to one-way bending conditions. Similarly, the selected masonry material properties did not differ from the ones experimentally-determined (see **Table 1**).

In the following, selected numerical collapse failure modes and predicted hysteretic curves are compared with their experimental counterparts (see **Fig. 7**), expressed in terms of OOP displacement against the corresponding OOP forces. As discussed above for the one-way tests, because of the differences in terms of experimental/numerical collapse PTAs, only "comparable data" are reported in the latter. It is also noted that, for space constraints, the calibration of the models when subjected to in-plane actions (which might be of relevance for the response of the return walls) has not been discussed in this work. Readers are thus referred to the dedicated publications by Malomo et al. (e.g. [37,38,54]).

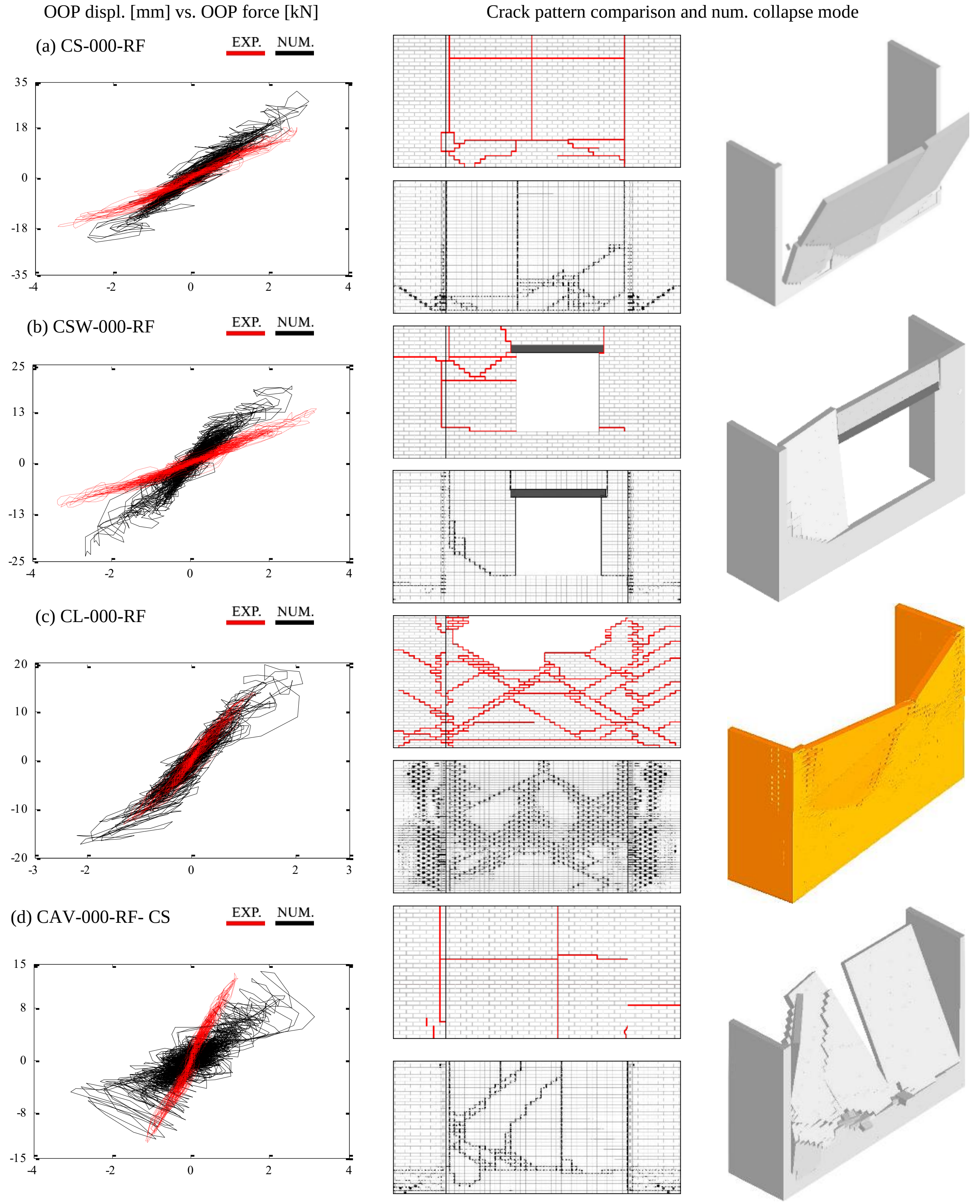

Fig. 7(a)(b)(c)(d) Exp. [12] vs. num. hysteresis and crack pattern (note: the colour used for the 3D images of the walls changes as a function of the wall material, where CS is grey and CL is orange)

The results above seem to confirm the capability of AEM in adequately capturing the OOP response of URM components subjected to two-way bending conditions, given that the models did reproduce in a relatively satisfactory manner both the failure modes of the specimens, as well as their hysteretic response in the pre-cracked range (especially considering that the OOP displacement values are very small, and consequently very sensitive to even the slightest of differences between the experimental and numerical deformed shapes). The stiffness of the CS specimens, on the other hand, is slightly overestimated. In the case of the cavity wall assembly (i.e. CAV-000-RF, **Fig. 7**(d)), seemingly spurious response cycles are observable in the numerical hysteresis envelopes shown in **Fig. 7**, as is an underestimation of the stiffness. This might be attributable to the above-described simplified modelling strategy adopted for simulating the dynamic interaction between masonry central OOP panels and tie elements; by precluding the modelling of the experimentally-observed interpenetration between ties and mortar bonds, spurious impact vibrations between the ties and the wall leaves are numerically generated. This notwithstanding, as in the case of the other specimens, an acceptable agreement in terms of cracks propagation was found, especially for the central panels.

Still, and again as was done also for the one-way tests, in **Fig. 8**(a) the full displacement capacity exhibited by the test specimens is compared with the numerical estimations. Because of the simplified joint and unit constitutive models implemented in the employed numerical tool (e.g. no post-peak softening behaviour is considered in shear and tension), when comparing the PTA at which collapses occurred experimentally with the ones predicted by the models, in some cases relevant differences were observed, as shown in **Fig. 8**(b). Such hypothesis is also supported by the fact that the numerical collapse was often reached in the immediately subsequent input sequence with respect to the one in which the activation of the failure mechanism was observed. In some specific cases (e.g. CL-000-RF), when the collapse predicted by the numerical models occurred for a loading stage different from their experimental counterparts, inducing a slightly different damage evolution (e.g. for the case of CL-000-RF only a partial collapse of the upper portion of the central panel occurred during the test, whilst the model predicted a full collapse of the panel), non-negligible dissimilarities were found.

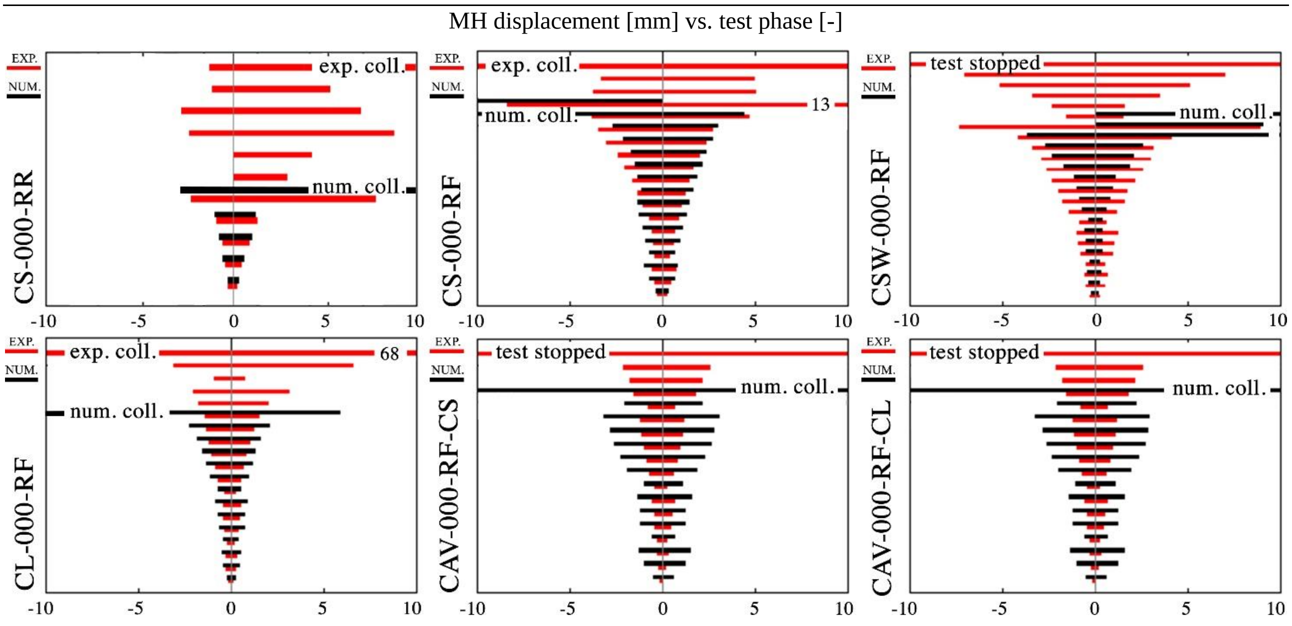

(a)

Specimen ID	Exp. mech. activation PTA [g]	Num. mech. PTA [g]	Exp. mech. collapse PTA [g]	Num. mech. collapse PTA [g]	Analysis time [h]
CS-005-RR	1.93	1.18	1.42	1.93	2.2
CS-000-RF	1.28	0.95	0.62	1.10	2.6
CSW-000-RF	1.28	0.65	0.91	1.13	1.8
CL-000-RF	1.11	0.76	1.71	0.94	3.1
CAV-000-RF	1.37	0.57	1.37	0.59	4.3

(b)

Fig. 8 Experimental (in red) vs. numerical (in black) results: MH displacement vs. test phase and exp. vs. num. activation mechanism and collapse PTA values

MODELLING THE OUT-OF-PLANE COLLAPSE OF A DYNAMICALLY-TESTED BUILDING PROTOTYPE

In this section, the modelling approach employed for the simulation of the wall components presented above is extended towards the simulation of the shake-table response of a full-scale building specimen, named LNEC-BUILD1, which has been tested at the laboratory of LNEC (Lisbon, Portugal), in the context of a wider experimental campaign [70]. LNEC-BUILD1 (see **Fig.9**(a)) was meant to represent the upper levels of EUC-BUILD1, namely a two-storey house prototype tested at the laboratory of Eucentre by Graziotti et al. [68]. These set of tests were aimed at assessing, among other aspects, the seismic capacity of low-rise cavity wall constructions (hereinafter referred as to *terraced houses*) in the Groningen region (The Netherlands), now exposed to induced seismicity due to gas extraction [71], typically designed without specific seismic considerations or detailing. This additional numerical exercise was undertaken with a view to investigate the effectiveness of the proposed modelling strategy when considering more complex and realistic boundary conditions and dynamic interactions among in-plane and OOP-loaded members, thus enabling a broader exploration and more accurate assessment of both potential limits and actual capabilities.

As comprehensively discussed in Tomassetti et al. [13], LNEC-BUILD1 consisted of a single-story full-scale prototype 5.82 m long, 5.46 m wide and 4.93 m high with a total mass of 31.7 tons, with cavity walls (2 ties/m^2), reinforced concrete (RC) floor diaphragm and pitched timber roof. The latter was constituted by one ridge beam, two 1.20 m-spaced joists per side among the ridge beam and two timber plates rigidly connected to the CS longitudinal walls. Timber planks (182x18 mm), covered by ceramic tiles (modelled as lumped masses), were placed on top using a couple of 60x2 mm steel nails. An incremental biaxial dynamic loading protocol (imposed along vertical and longitudinal direction), representative of the first-floor accelerations recorded during EUC-BUILD1 shake-table test, was applied till collapse of the specimen. To this end, two different input motions (i.e. *FEQ1* and *FEQ2,* progressively scaled from 50 up to 150% and from 50 up to 300% respectively), whose corresponding signals and PTA are shown in **Fig.9**(b), were considered.

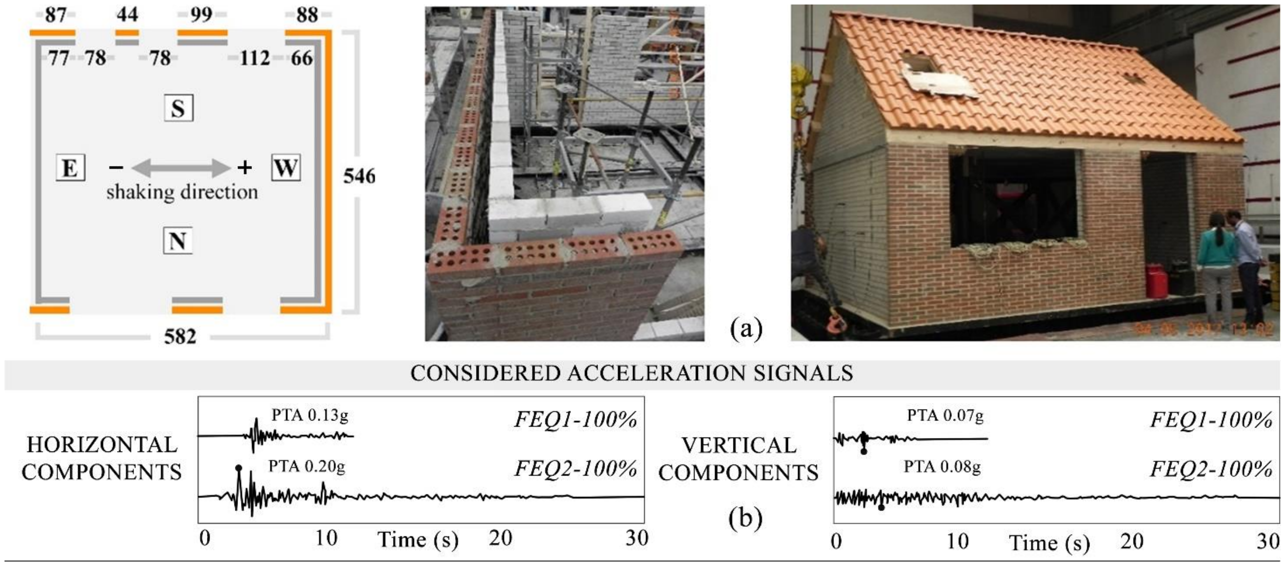

Fig. 9 (a) Plan (in cm) and experimental configuration of LNEC-BUILD1 [13], (b) *FEQ1 and FEQ2* acceleration time-histories

While the idealisation of the roof system, which featured the representation of each component of the flexible diaphragms (i.e. planks and joists), as well as the selection and calibration of the associated mechanical properties, is presented elsewhere (i.e. [38]), special attention will be given in what follows to the modelling of the interaction among URM elements (whose mechanical properties are reported in **Table 3**), and, more precisely, to the numerical representation of the experimentally-observed OOP-governed collapse mode of the CS East party wall (see **Fig.9**(a)). As can be gathered by the latter figure, the CL veneer was not present on the East side (i.e. where the experimental collapse occurred), because the specimen was meant to represent the end-unit of a set of terraced houses.

Table 3 Experimental [13] and inferred material properties of both CS and CL brick masonry

	CS - density δ_m = 1800 [kg/m^3]								CL - density δ_m = 1839 [kg/m^3]							
	fc_m	fc_u	f_w	E_m	c	μ [-]	E_u	E_{mo}	fc_m	fc_u	f_w	E_m	c	μ [-]	E_u	E_{mo}
Avg [MPa]	9.8	16.3	0.4	7955	0.4	0.5	8990	4537	19.4	32.5	0.2	13118	0.4	0.8	7211	3332
C.o.V. [%]	0.1	0.1	0.2	0.2	-	-	0.4	-	0.1	0.1	0.5	0.1	-	-	0.2	-

Prior to the *FEQ-300%* (i.e. final test phase), the response was mainly governed by the flexural/rocking modes of the longitudinal CS slender piers. Then, during *FEQ2-300%*, the progressive increase in their displacement demand led to an important uplift of the RC slab which in turn triggered the OOP collapse of the consequently no longer vertically loaded CS transverse panel (see [13]).

In **Fig.10**, a comparison between experimental and predicted hysteretic response (starting from *FEQ1-150%*, i.e. when nonlinear response became predominant), expressed in the form of attic floor horizontal displacement vs. total base shear, is proposed. It is recalled that further details concerning the performance of the model with respect to the roof level are presented in [38], to which interested readers are thus referred.

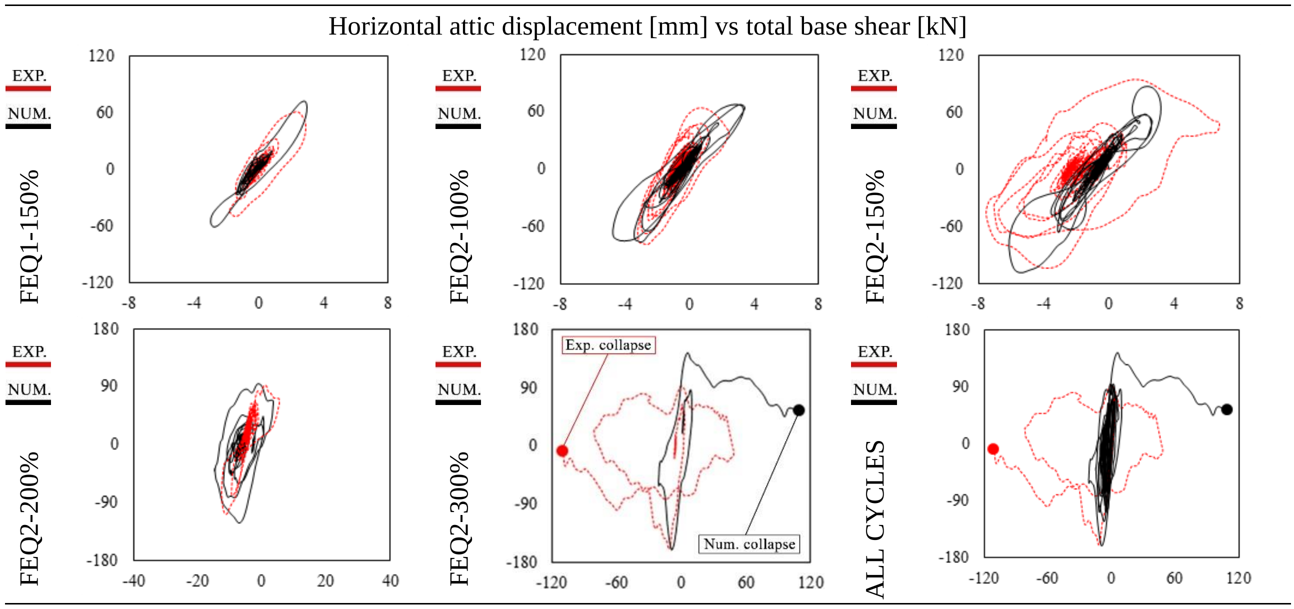

Fig. 10 Exp. [13] vs num. (a) attic-floor hysteretic response

The response predicted by the model appears in rather good agreement with the one exhibited by the specimen, both in terms of overall capacity and displacement demand, though the energy dissipation was not always fully captured, especially during *FEQ2-150%*. With reference to the displacement capacity prediction, major differences were also found in the last test phase. This aspect might be related to the fact that collapse occurred at *FEQ2-300%*, possibly influencing the associated maximum attic and roof deformations in the final cycles. Nonetheless, as shown in **Fig.11**(a), the global damage evolution was captured in a relatively satisfactory manner. Of particular interest is the fact that most of the experimentally-observed local failure modes depicted in **Fig.11**(b), and mainly attributable to various dynamic interactions among in-plane and OOP-loaded components, has been satisfactorily reproduced by the model.

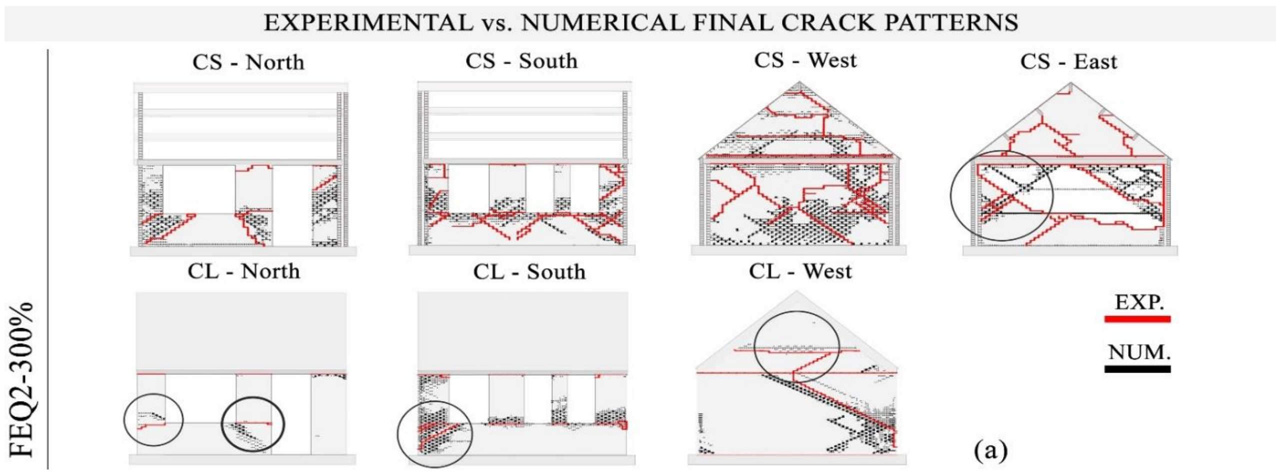

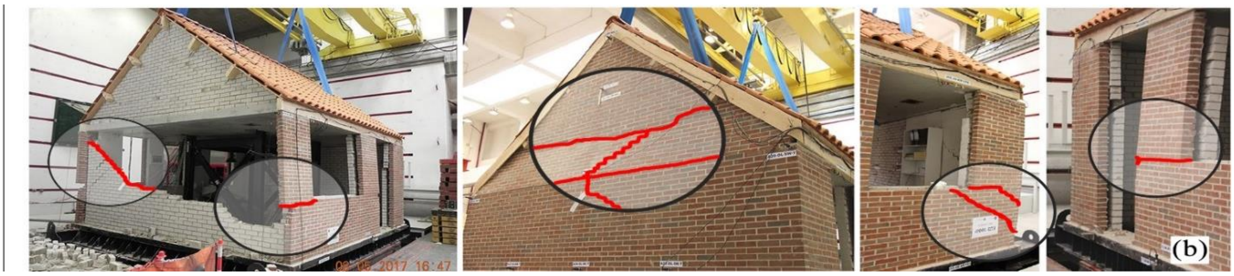

Fig. 11 (a) Exp. [13] vs. num. crack pattern and (b) local in-plane and OOP exp. failure modes

Further, and again comparing the numerical results presented in this section with those related to the simulation of wall assemblies alone, it is worth noting that the possibility of describing in a more realistic way the interaction between in-plane and OOP-loaded members, also in terms of boundary conditions, led to an enhanced representation of both experimental displacement capacity and local damage, without any visible effect or impact of the previously discussed spurious high-frequency vibrations. Moreover, the numerical model was herein able to simulate the response of OOP-loaded members almost until the end of the actual loading sequence. Indeed, numerical collapse (see **Fig.12**(a)) occurred slightly before the actual experimental one, which may also explain the differences, as mentioned above, in the hysteresis curves of *FEQ2-300%*. The latter was herein simply identified from analysis results by visually comparing the evolution of the predicted collapse mechanism of the considered structural member with its experimental counterpart. For the sake of simplicity, the analyses were subsequently interrupted once the monitored URM component was not able to carry vertical load anymore.

In this connection, as illustrated in **Fig.12(b)**, the model was also able to account explicitly for the interaction between the CS longitudinal piers and the RC slab, resulting in an adequate representation of the OOP collapse of the East CS wall induced by the diaphragm uplift, which had a maximum value of 28 mm in the numerical model. Although it was not measured experimentally, the model prediction is close to the analytically-inferred value of 25 mm proposed by Tomassetti et al. [13].

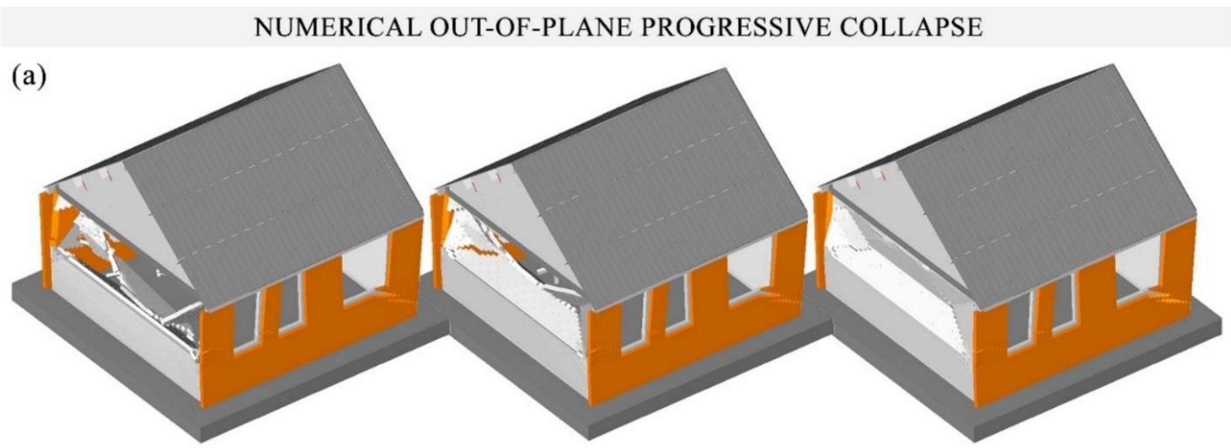

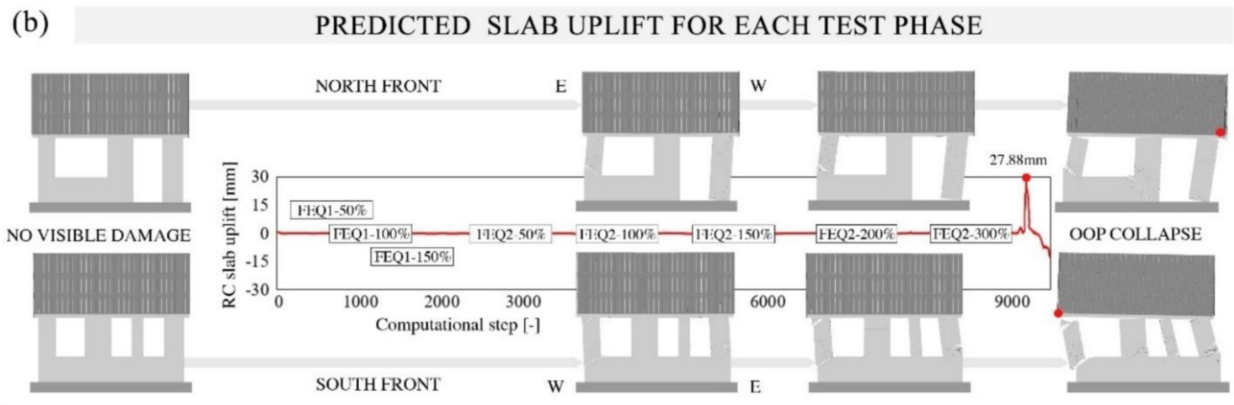

Fig.12 (a) Numerical progressive collapse of the East CS party wall and (b) predicted slab uplift

CONCLUSIONS

Since relatively limited work has over the years been carried out on the verification and validation of numerical approaches for modelling brick masonry walls (in both single leaf and cavity wall configurations) when subjected to OOP seismic input, an attempt was made in this endeavour to address the aforementioned knowledge gap by simulating a series of shake-table tests on full-scale URM wall specimens (under both one- and two-way bending conditions). Use was made of the Applied Element Method (AEM), which was thus scrutinised and consequently verified in this work through comparison against laboratory test results. With a view to investigate further both potential limits and actual capabilities of the adopted modelling strategy, its application was also extended to the simulation of the dynamic response of a full-scale one-story cavity wall house prototype, whose complex OOP collapse was significantly influenced by the dynamic interaction with the surrounding in-plane-loaded components.

The analyses results seem to indicate a capability of the AEM to satisfactorily capture both the crack pattern and the collapse mode of the considered set of full-scale URM assemblies. Nonetheless, further improvements to the proposed modelling approach are currently being explored to try to address some of the shortcomings discussed in this paper, and in particular the observed difficulties in adequately capturing the stiffness of some of the tested walls and to enhance the representation of tie-to-wall dynamic interaction. Moreover, although a good agreement was found in terms of collapse acceleration, the models often provided conservative estimates of the actual ultimate capacity of the considered specimens. However, when applying the same modelling strategy to the simulation of a full building specimen, the impact of most of these modelling difficulties tends to vanish. Indeed, in such final modelling exercise, a more accurate representation of both hysteretic response and collapse mode, as well as an improved description of local OOP damage, was obtained. As shown by the comparison among experimental and numerical crack propagation, the interaction between in-plane and OOP modes was also captured adequately, resulting in a satisfactory representation of the OOP collapse of the East CS wall induced by the diaphragm uplift. From these investigations, it can be thus concluded that:

- The AEM is capable of modelling of OOP-governed responses of URM components, especially in the pre-cracked range. Once major damage occurs, the models tend to underestimate the actual OOP capacity.
- This aspect is more evident when simulating the dynamic OOP behaviour of wall specimens, i.e. where experimental layouts feature "idealised" boundary conditions and *a priori*-defined overburden pressures. In this case, the simplified idealisation of tie elements, necessary to avoid a detailed modelling of pull-in and pull-out failure modes (e.g. representing explicitly interpenetration phenomena and associated damage, which would significantly increase computational expense), might lead to spurious high-frequency impact vibrations generated at the tie-to-wall interface.
- This notwithstanding, a good agreement in terms of crack pattern can be found without the need of adjusting the experimentally-measured material properties. For responses in which cracks are expected to propagate through bricks, however, the introduction of additional subdivisions within unit elements is recommended.
- As already mentioned, when considering full-scale building prototypes, which typically entail the definition of more realistic boundary conditions spontaneously defined by the interaction among adjacent members, most of the abovementioned difficulties tend to vanish.
- Nonetheless, the employment of a simplified tension cut-off criterion (as a result of which most of the actual collapse capacities, especially in the case of two-way bending, were underestimated), typically implemented in discontinuum-based codes and according to which the interface strength is automatically set to zero after reaching the maximum input value (thus neglecting any residual capacity), might lead to an underestimation of dissipated energy. In this connection, with a view to further investigate the influence of the abovementioned simplified assumptions on numerical accuracy, and to determine on a case-by-case basis whether they are acceptable or not, it would be also interesting to compare the obtained results with those inferred using different interface-based approaches characterised by more refined joint constitutive laws (e.g. [33,72–74]), perhaps also considering additional structural configurations (e.g. with different diaphragm systems, chimneys) and masonry types.

- The AEM appear suitable for the simulation of the global response of URM structures, up to complete collapse, even when OOP modes are predominant and in cases when the effects of the interaction among in-plane and OOP-loaded members are expected to play a relevant role.

Future improvements may include the introduction of enhanced constitutive laws at the joint level, thus accounting for the experimentally-observed post-peak softening branch in tension, as well as the development of a more effective modelling strategy for representing the dynamic interaction between tie elements and masonry members.

ACKNOWLEDGEMENTS

The work described in this paper was carried out within the framework of the research program on hazard and risk of induced seismicity in the Groningen region, sponsored by the Nederlandse Aardolie Maatschappij BV (NAM). The authors acknowledge all those at the European Centre for Training and Research in Earthquake Engineering (EUCENTRE, Pavia, Italy) that were involved in the testing campaign referred to in this paper, and in particular Francesco Graziotti, Satyadhrik Sharma, Luca Grottoli and Umberto Tomassetti, for their precious assistance in accessing the test data. The authors would also like to thank Paolo Comini, whose valuable contribution to the development of the numerical models is deeply appreciated. The collaboration of the technical support staff from Applied Science International LLC (ASI), on the use of the employed AEM software - Extreme Loading for Structures, is also acknowledged. Finally, the authors would like to express their gratitude to three anonymous reviewers, whose pertinent and constructive feedback on the initial version of the manuscript helped improving its contents significantly.

REFERENCES

[1] Sorrentino L, Cattari S, da Porto F, Magenes G, Penna A. Seismic behaviour of ordinary masonry buildings during the 2016 central Italy earthquakes. Bull Earthq Eng 2018:1–25. doi:10.1007/s10518-018-0370-4.

[2] Penna A, Morandi P, Rota M, Manzini CF, Da Porto F, Magenes G. Performance of masonry buildings during the Emilia 2012 earthquake. Bull Earthq Eng 2014;12:2255–73.

[3] Ingham J, Griffith M. Performance of unreinforced masonry buildings during the 2010 Darfield (Christchurch, NZ) earthquake. Aust J Struct Eng 2011;11:207–24. doi:10.1080/13287982.2010.11465067.

[4] Sorrentino L, D'Ayala D, de Felice G, Griffith MC, Lagomarsino S, Magenes G. Review of Out-of-Plane Seismic Assessment Techniques Applied To Existing Masonry Buildings. Int J Archit Herit 2017;11:2–21. doi:10.1080/15583058.2016.1237586.

[5] Maccarini H, Vasconcelos G, Rodrigues H, Ortega J, Lourenço PB. Out-of-plane behavior of stone masonry walls: Experimental and numerical analysis. Constr Build Mater 2018;179:430–52. doi:10.1016/j.conbuildmat.2018.05.216.

[6] Griffith MC, Vaculik J, Lam NTK, Wilson J, Lumantarna E. Cyclic testing of unreinforced masonry walls in two-way bending. Earthq Eng Struct Dyn 2007;36:801–21. doi:10.1002/eqe.654.

[7] Derakhshan H, Lucas W, Visintin P, Griffith MC. Out-of-plane Strength of Existing Two-way Spanning Solid and Cavity Unreinforced Masonry Walls. Structures 2018;13:88–101. doi:10.1016/j.istruc.2017.11.002.

[8] Restrepo Vélez LF, Magenes G, Griffith MC. Dry stone masonry walls in bending-Part I: Static tests. Int J Archit Herit 2014;8:1–28. doi:10.1080/15583058.2012.663059.

[9] Vaculik J, Griffith MC. Out-of-plane shaketable testing of unreinforced masonry walls in two-way bending. Bull Earthq Eng 2017:1–38. doi:10.1007/s10518-017-0282-8.

[10] Costa AA, Arêde A, Costa AC, Penna A, Costa A. Out-of-plane behaviour of a full scale stone masonry façade. Part 1: Specimen and ground motion selection. Earthq Eng Struct Dyn 2013;42:2081–95. doi:10.1002/eqe.2313.

[11] Candeias PX, Campos Costa A, Mendes N, Costa AA, Lourenço PB. Experimental Assessment of the Out-of-Plane Performance of Masonry Buildings Through Shaking Table Tests. Int J Archit Herit 2017;11:31–58. doi:10.1080/15583058.2016.1238975.

[12] Graziotti F, Tomassetti U, Sharma S, Grottoli L, Magenes G. Experimental response of URM single leaf and cavity walls in out-of-plane two-way bending generated by seismic excitation. Constr Build Mater 2019;195:650–70. doi:10.1016/j.conbuildmat.2018.10.076.

[13] Tomassetti U, Correia AA, Candeias PX, Graziotti F, Campos Costa A. Two-way bending out-of-plane collapse of a full-scale URM building tested on a shake table. Bull Earthq Eng 2019;17:2165–98. doi:10.1007/s10518-018-0507-5.

[14] Mendes N, Costa AA, Lourenço PB, Bento R, Beyer K, de Felice G, et al. Methods and Approaches for Blind Test Predictions of Out-of-Plane Behavior of Masonry Walls: A Numerical Comparative Study. Int J Archit Herit 2017;11:59–71. doi:10.1080/15583058.2016.1238974.

[15] Cundall PA. A computer model for simulating progressive large-scale movements in blocky rock systems. Proc. Symp. Int. Soc. Rock Mech., vol. 1, Nancy, France: 1971, p. No. 8.

[16] Bui TT, Limam A, Sarhosis V, Hjiaj M. Discrete element modelling of the in-plane and out-of-plane behaviour of dry-joint masonry wall constructions. Eng Struct 2017;136:277–94.

[17] Lemos J V. Discrete element modeling of masonry structures. Int J Archit Herit 2007;1:190–213.

[18] Galvez F, Segatta S, Giaretton M, Walsh K, Giongo I, Dizhur D. FE and DE modelling of out-of-plane two way bending behaviour of unreinforced masonry walls. 16th Eur. Conf. Earthq. Eng., Thessaloniki, Greece: 2018.

[19] Pulatsu B, Bretas EM, Lourenço PB. Discrete element modeling of masonry structures: Validation and application. Earthq Struct 2016;11:563–82. doi:10.12989/eas.2016.11.4.563.

[20] Godio M, Beyer K. Evaluation of force-based and displacement-based out-of-plane seismic assessment methods for unreinforced masonry walls through refined model simulations. Earthq Eng Struct Dyn 2019;48:454–75. doi:10.1002/eqe.3144.

[21] Akhaveissy AH, Desai CS. Unreinforced Masonry Walls: Nonlinear Finite Element Analysis with a Unified Constitutive Model. Arch Comput Methods Eng 2011;18:485–502. doi:10.1007/s11831-011-9067-4.

[22] Nazir S, Dhanasekar M. Modelling the failure of thin layered mortar joints in masonry. Eng Struct 2013;49:615–27. doi:10.1016/j.engstruct.2012.12.017.

[23] Nazir S, Dhanasekar M. A non-linear interface element model for thin layer high adhesive mortared masonry. Comput Struct 2014;144:23–39. doi:10.1016/j.compstruc.2014.07.023.

[24] Portioli FPA. Rigid block modelling of historic masonry structures using mathematical programming: a unified formulation for non-linear time history, static pushover and limit equilibrium analysis. Bull Earthq Eng 2019:1–29. doi:10.1007/s10518-019-00722-0.

[25] de Felice G. Out-of-plane seismic capacity of masonry depending on wall section morphology. Int J Archit Herit 2011;5:466–82. doi:10.1080/15583058.2010.530339.

[26] Lemos J V., Campos Costa A. Simulation of Shake Table Tests on Out-of-Plane Masonry Buildings. Part (V): Discrete Element Approach. Int J Archit Herit 2017;11:117–24. doi:10.1080/15583058.2016.1237587.

[27] Galvez F, Giaretton M, Abeling S, Ingham J, Dizhur D. Discrete Element modelling of a two-storey unreinforced masonry scaled model. 16th Eur. Conf. Earthq. Eng., Thessaloniki, Greece: 2018.

[28] Kawai T. New discrete models and their application to seismic response analysis of structures. Nucl Eng Des 1978;48:207–29.

[29] Casolo S. A numerical study on the cumulative out-of-plane damage to church masonry façades due to a sequence of strong ground motions. Earthq Eng Struct Dyn 2017;46:2717–37. doi:10.1002/eqe.2927.

[30] Furukawa A, Kiyono J, Toki K. Numerical simulation of the failure propagation of masonry buildings during an earthquake. J Nat Disaster Sci 2012;33:11–36.

[31] Silva LC, Lourenço PB, Milani G. Nonlinear Discrete Homogenized Model for Out-of-Plane Loaded Masonry Walls. J Struct Eng 2017;143:04017099. doi:10.1061/(ASCE)ST.1943-541X.0001831.

[32] Baraldi D, Cecchi A. A full 3D rigid block model for the collapse behaviour of masonry walls. Eur J Mech A/Solids 2017;64:11–28. doi:10.1016/j.euromechsol.2017.01.012.

[33] Pantò B, Cannizzaro F, Caliò I, Lourenço PB. Numerical and Experimental Validation of a 3D Macro-Model for the In-Plane and Out-Of-Plane Behavior of Unreinforced Masonry Walls. Int J Archit Herit 2017;11:946–64. doi:10.1080/15583058.2017.1325539.

[34] Meguro K, Tagel-Din H. Applied element method for structural analysis: Theory and application for linear materials. Struct Eng Eng 2000;17:21s--35s.

[35] Meguro K, Tagel-Din H. Applied Element Method Used for Large Displacement Structural Analysis. J Nat Disaster Sci 2002;24:25–34.

[36] Meguro K, Tagel-Din H. Applied Element Simulation of RC Structures under Cyclic Loading. J Struct Eng 2001;127:1295–305. doi:10.1061/(ASCE)0733-9445(2001)127:11(1295).

[37] Malomo D, Pinho R, Penna A. Applied Element Modelling of the Dynamic Response of a Full-Scale Clay Brick Masonry Building Specimen with Flexible Diaphragms. Int J Archit Herit 2019:1–18. doi:10.1080/15583058.2019.1616004.

[38] Malomo D, Pinho R, Penna A. Simulating the shake-table response of URM cavitywall structures tested to collapse or near-collapse conditions. Earthq Spectra 2020. https://doi.org/10.1177/8755293019891715. in press.

[39] Calvi GM, Moratti M, O'Reilly GJ, Scattarreggia N, Monteiro R, Malomo D, et al. Once upon a Time in Italy: The Tale of the Morandi Bridge. Struct Eng Int 2019;29:198–217. doi:10.1080/10168664.2018.1558033.

[40] Karbassi A, Nollet M-J. Performance-based seismic vulnerability evaluation of masonry buildings using applied element method in a nonlinear dynamic-based analytical procedure. Earthq Spectra 2013;29:399–426.

[41] Domaneschi M, Cimellaro GP, Scutiero G. A simplified method to assess generation of seismic debris for masonry structures. Eng Struct 2019;186:306–20. doi:10.1016/j.engstruct.2019.01.092.

[42] Adhikari R, D'Ayala D. Numerical Seismic Performance Assessment of Pre-Earthquake Stone Masonry Residential Building Typology in Light of 2015 Nepal Earthquake. Proc. Soc. Earthq. Civ. Eng. Dyn. Conf., Greenwich, London: SECED (Society for Earthquake and Civil Engineering Dynamics); 2019.

[43] Applied Science International LLC. Extreme Loading for Structures (2018) 2018.

[44] Graziotti F, Tomassetti U, Penna A, Magenes G. Out-of-plane shaking table tests on URM single leaf and cavity

walls. Eng Struct 2016;125:455–70.

[45] Crowley H, Polidoro B, Pinho R, Van Elk J. Framework for developing fragility and consequence models for local personal risk. Earthq Spectra 2017;33:1325–45. doi:10.1193/083116EQS140M.

[46] Crowley H, Pinho R, van Elk J, Uilenreef J. Probabilistic damage assessment of buildings due to induced seismicity. Bull Earthq Eng 2018. doi:10.1007/s10518-018-0462-1.

[47] Malomo D, DeJong MJ, Penna A. Distinct element modelling of the in-plane cyclic response of URM walls subjected to shear-compression. Earthq Eng Sructural Dyn 2019;48(12):1322–44. https://doi.org/10.1002/eqe.3178.

[48] Jäger W, Irmschler H, Schubert P. Mauerwerk-Kalender 2004. Ernst & Sohn Verlag für Architektur und technische Wissenschaften; 2004.

[49] Kaushik HB, Rai DC, Jain SK. Stress-strain characteristics of clay brick masonry under uniaxial compression. J Mater Civ Eng 2007;19:728–39.

[50] Brooks JJ, Baker A. Modulus of Elasticity of Masonry. Mason Int 1998;12:58–63.

[51] Matysek P, Janowski Z. Analysis of factors affecting the modulus of elasticity of the walls. Proc. Conf. Comm. Civ. Eng. PZITB Lublin, Pol., 1996.

[52] Ciesielski R. The dynamic module of elasticity of brick walls. Proc. Conf. Comm. Civ. Eng. PZITB Lublin, Pol., 1999.

[53] U.B.C. International Conference of Building Officials. Uniform Building Code. Int. Conf. Build. Off. USA, Whittier, USA: 1991.

[54] Malomo D, Pinho R, Penna A. Using the applied element method for modelling calcium silicate brick masonry subjected to in-plane cyclic loading. Earthq Eng Struct Dyn 2018;47:1610–30. doi:10.1002/eqe.3032.

[55] El-Kashif KF, Maekawa K. Time-dependent nonlinearity of compression softening in concrete. J Adv Concr Technol 2004;2:233–47.

[56] Psycharis IN, Fragiadakis M, Stefanou I. Seismic reliability assessment of classical columns subjected to near-fault ground motions. Earthq Eng Struct Dyn 2013;42:2061–79. doi:10.1002/eqe.2312.

[57] Malomo D, Pinho R, Penna A. The Applied Element Method and the modelling of both in-plane and out-of-plane resposne of URM walls. 16th Eur. Conf. Earthq. Eng., Thessaloniki, Greece: 2018.

[58] Tagel-Din H. A new efficient method for nonlinear, large deformation and collapse analysis of structures. Dr Thesis, Univ Tokyo 1998.

[59] Malomo D, Scattarreggia N, Pinho R, Moratti M, Calvi GM. Numerical study on the collapse of the Morandi bridge. J Perform Constr Facil - Accepted for publication, 2019.

[60] Jafari S, Rots JG, Esposito R, Messali F. Characterizing the Material Properties of Dutch Unreinforced Masonry. Procedia Eng 2017;193:250–7. doi:10.1016/j.proeng.2017.06.211.

[61] Graziotti F, Tomassetti U, Sharma S, Grottoli L, Magenes G. Experimental response of URM single leaf and cavity walls in out-of-plane two-way bending generated by seismic excitation. Constr Build Mater 2019;195:650–70. doi:10.1016/j.conbuildmat.2018.10.076.

[62] Tomassetti U, Grottoli L, Sharma S, Graziotti F. Dataset from dynamic shake-table testing of five full-scale single leaf and cavity URM walls subjected to out-of-plane two-way bending. Data Br 2019;24:103854. doi:10.1016/j.dib.2019.103854.

[63] Messali F, Esposito R, Maragna M. Pull-out strength of wall ties. Report, TU Delft, NL 2016.

[64] Bourne SJ, Oates SJ, Bommer JJ, Dost B, Van Elk J, Doornhof D. A monte carlo method for probabilistic hazard

assessment of induced seismicity due to conventional natural gas production. Bull Seismol Soc Am 2015;105:1721–38. doi:10.1785/0120140302.

[65] Lagomarsino S, Penna A, Galasco A, Cattari S. TREMURI program: an equivalent frame model for the nonlinear seismic analysis of masonry buildings. Eng Struct 2013;56:1787–99.

[66] Tomassetti U, Graziotti F, Penna A, Magenes G. Modelling one-way out-of-plane response of single-leaf and cavity walls. Eng Struct 2018;167:241–55. doi:10.1016/j.engstruct.2018.04.007.

[67] Kallioras S, Graziotti F, Penna A. Numerical assessment of the dynamic response of a URM terraced house exposed to induced seismicity. Bull Earthq Eng 2019;17:1521–52. doi:10.1007/s10518-018-0495-5.

[68] Graziotti F, Tomassetti U, Kallioras S, Penna A, Magenes G. Shaking table test on a full scale URM cavity wall building. Bull Earthq Eng 2017;15:5329–64. doi:10.1007/s10518-017-0185-8.

[69] Graziotti F, Tomassetti U, Rossi A, Kallioras S, Mandirola M, Cenja E, et al. Experimental campaign on cavity wall systems representative of the Groningen building stock - Report n. EUC318/2015U. Pavia, Italy: 2015.

[70] Graziotti F, Penna A, Magenes G. A comprehensive in situ and laboratory testing programme supporting seismic risk analysis of URM buildings subjected to induced earthquakes. Bull Earthq Eng 2019;17:4575–99. doi:10.1007/s10518-018-0478-6.

[71] van Elk J, Bourne SJ, Oates SJ, Bommer JJ, Pinho R, Crowley H. A Probabilistic Model to Evaluate Options for Mitigating Induced Seismic Risk. Earthq Spectra 2019:050918EQS118M. doi:10.1193/050918EQS118M.

[72] Pulatsu B, Erdogmus E, Lourenço PB, Quey R. Simulation of uniaxial tensile behavior of quasi-brittle materials using softening contact models in DEM. Int J Fract 2019;217:105–25. doi:10.1007/s10704-019-00373-x.

[73] D’Altri AM, Messali F, Rots J, Castellazzi G, de Miranda S. A damaging block-based model for the analysis of the cyclic behaviour of full-scale masonry structures. Eng Fract Mech 2019;209:423–48. doi:10.1016/j.engfracmech.2018.11.046.

[74] Chácara C, Mendes N, Lourenço PB. Simulation of Shake Table Tests on Out-of-Plane Masonry Buildings. Part (IV): Macro and Micro FEM Based Approaches. Int J Archit Herit 2017;11:103–16. doi:10.1080/15583058.2016.1238972.